Taylor & Francis
Taylor & Francis Group

BASIC RESEARCH PAPER

🔓 OPEN ACCESS | Check for updates

Discovery of pan autophagy inhibitors through a high-throughput screen highlights macroautophagy as an evolutionarily conserved process across 3 eukaryotic kingdoms

Piyush Mishra[a], Adrian N. Dauphinee[b], Carl Ward[c], Sovan Sarkar[c], Arunika H.L.A.N. Gunawardena[b], and Ravi Manjithaya[a]

[a]Molecular Biology and Genetics Unit, Jawaharlal Nehru Centre for Advanced Scientific Research, Jakkur, Bangalore, India; [b]Biology Department, Life Sciences Centre, Dalhousie University, Halifax, NS, Canada; [c]Institute of Cancer and Genomic Sciences, Institute of Biomedical Research, College of Medical and Dental Sciences, University of Birmingham, Edgbaston, Birmingham, UK

ABSTRACT

Due to the involvement of macroautophagy/autophagy in different pathophysiological conditions such as infections, neurodegeneration and cancer, identification of novel small molecules that modulate the process is of current research and clinical interest. In this work, we developed a luciferase-based sensitive and robust kinetic high-throughput screen (HTS) of small molecules that modulate autophagic degradation of peroxisomes in the budding yeast *Saccharomyces cerevisiae*. Being a pathway-specific rather than a target-driven assay, we identified small molecule modulators that acted at key steps of autophagic flux. Two of the inhibitors, Bay11 and ZPCK, obtained from the screen were further characterized using secondary assays in yeast. Bay11 inhibited autophagy at a step before fusion with the vacuole whereas ZPCK inhibited the cargo degradation inside the vacuole. Furthermore, we demonstrated that these molecules altered the process of autophagy in mammalian cells as well. Strikingly, these molecules also modulated autophagic flux in a novel model plant, *Aponogeton madagascariensis*. Thus, using small molecule modulators identified by using a newly developed HTS autophagy assay, our results support that macroautophagy is a conserved process across fungal, animal and plant kingdoms.

Introduction

Macroautophagy (generally referred to as autophagy) is an evolutionarily conserved process from yeast to humans.[1] The process involves engulfment of intracellular components inside double-membrane vesicles called autophagosomes and subsequent degradation by the lysosomal machinery.[2] The degradation products, such as amino acids and other basic building blocks, are recycled back to the cytoplasm and are used up by the cell.[3,4] Other than bulk degradation of cytoplasmic contents, autophagy is also involved in selective degradation of aggregated proteins (aggrephagy), excess or damaged organelles such as mitochondria (mitophagy), peroxisomes (pexophagy) and intracellular pathogens (xenophagy).[5]

A constitutive level of basal autophagy maintains the cellular homeostasis under normal growth conditions.[6,7] Its dysfunction causes accumulation of damaged organelles and misfolded protein aggregates that can be cytotoxic, ultimately leading to pathological conditions such as cancer, neurodegeneration and other diseases.[8] In cancer, the role of autophagy is context-dependent and the situation is commonly referred to as 'a double edged sword.'[9,10] In the case of most neurodegenerative diseases, accumulation of toxic misfolded protein aggregates is seen in conjunction with impaired autophagy.[11,12]

Since dysfunction of autophagy leads to a plethora of diseases, genetic and pharmacological modulation of autophagy is a promising approach for treatment.[13] For example, silencing of core autophagy genes such as *ATG5* inhibits tumor growth of human pancreatic cancer cells in a mouse xenograft model.[13] In addition, modulating autophagic activity results in increased killing of intracellular pathogens including mycobacteria,[14] *Salmonella*,[15] *Shigella*[16] and group A *Streptococcus*.[17] Pharmacologically, small molecules stimulating autophagy are effective in clearing protein aggregates in mouse models of Huntington disease and other neurodegenerative disorders.[18-20] Several studies have reported the discovery of novel or repurposed drugs for restoring autophagy balance.[21] For example, small-molecule enhancers and inhibitors of autophagy have been identified using a phenotypic high-throughput screen (HTS) based on chemical genetics and proteome chips.[22] In some of these studies, distinct assays are used for a HTS to identify small molecules that modulate autophagy.[23-26]

Keeping this rationale in mind, we developed a luciferase-based pexophagy assay in the yeast *S. cerevisiae* that allows measurement of autophagic cargo clearance rather than MAP1LC3B based changes in autophagosome number. Compared with the low turnover rates of cytoplasmic flux, the

autophagic turnover of an organelle such as the peroxisome can be easily monitored.[27] The advantage of using a peroxisome marker is that the cargo can build up and the degradation through autophagy can be followed over time.[28-30] Firefly luciferase-loaded peroxisomes,[31] when degraded in bulk, give a dramatic decrease in luciferase activity and a higher range to work with. Calculation of statistical parameters such as Z-factor showed that the assay is highly suitable for small molecule screening and that the assay would be useful in a HTS setting.

Here we show a kinetic and sensitive luciferase-based HTS assay in live yeast cells that monitor pexophagy. Employing this assay, we screened a small molecule library comprising of FDA-approved compounds. The autophagy inhibitors and enhancers selected from our screen affected various stages of autophagosome biogenesis and maturation. In this study, we focused on 2 potent autophagy inhibitors. Owing to the conserved nature of autophagy, we were interested to investigate whether the compounds affected autophagy across different kingdoms. We show that the small molecule inhibitors obtained from the HTS in yeast also modulated autophagy in mammalian cells and the novel lace plant (*Aponogeton madagascariensis*) model system.

Results

A novel high-throughput assay for monitoring autophagy in real time

The principle of the assay involves triggering the biogenesis of firefly luciferase cloned under an inducible promoter for a peroxisome-resident protein, *Saccharomyces cerevisiae* Pot1 (peroxisomal thiolase). This protein functions in the conversion of 3-ketoacyl-CoA into acyl-CoA and acetyl-CoA during β-oxidation of fatty acids.[32] Firefly luciferase is tagged at C-terminal with the 3 amino acid long peroxisomal targeting sequence (PTS1), SKL.[31] This targets firefly luciferase to the peroxisomes. Compared with the assay involving degradation of long-lived proteins, pexophagy based assays allow the buildup of cargo and degradation upon autophagy stimulation.[27,28] Peroxisome content is then built up inside the cell by culturing in fatty acid medium. Once the cargo builds up inside the cell, autophagy is triggered by transferring the cells to the starvation medium after which the degradation of luciferase marker is monitored over time. In this context, a decrease in the firefly luciferase activity would reflect selective degradation of peroxisomes (pexophagy) (Fig. 1A).

In the luciferase assay, the activity for the wild-type cells goes down with time whereas the autophagy mutant (*atg1Δ*) showed no decrease (Fig. 1B). The assays done at flask level showed an expected decrease in the levels of firefly luciferase activity upon autophagy induction (data not shown). Further, assays were standardized for 96- and 384-well formats using a fully automated system. Because the luciferase assay could be scaled down to a plate format and for shorter time durations, it enabled HTS studies for the identification of small molecule modulators of autophagy. Treatment with rapamycin, a known enhancer of autophagy, showed an expected increase in the rate of decay of firefly luciferase activity as also displayed by nutrient starvation conditions (SD-N) as compared with nutrient-rich (SD+N) conditions (Fig. 1C). The Z-factor, a measure of

quality of the HTS assay, was calculated to be 0.8628 ± 0.03481 for firefly luciferase from 5 independent assays performed in triplicates in a 384-well format. While the wild-type cells showed a gradual decrease in luciferase counts upon induction of autophagy (Fig. 1B-E), the core autophagy mutants *atg1Δ* (Fig. 1B) and *atg5Δ* (Fig. 1D) as well as the selective autophagy mutant *atg36Δ* (lacking a receptor protein for pexophagy) (Fig. 1E) did not show any drop in the luciferase activity over time. Our data suggest that selective degradation of firefly luciferase-laden peroxisomes occurs specifically through autophagy and not via any other intracellular degradation pathways.

Screening of small molecule libraries identified several putative modulators of autophagy

After validation of the luciferase assay, the Sigma library of pharmacologically active compounds (LOPAC) comprising of 1280 compounds including FDA-approved drugs were screened for their ability to affect autophagy. The rates of degradation of the untreated cells were compared with those treated with a 50 μM concentration of each of the small molecules. The time taken for 50% decrease in cargo activity (firefly luciferase activity) was compared between the untreated cells and the ones treated with individual compounds (Fig. 2A). A 3 standard deviation (SD) parameter was used as a criterion to obtain the hits from the primary screen. There were several hits, both inhibitors and enhancers identified from the primary screen (Table 1). The screen also identified several known modulators of autophagy, which further highlights the sensitivity and validates the assay in a HTS setup (Fig. 2B). Two of the potent inhibitors identified from the screen Bay11-7082 (Bay11) and Z-L-phenyl chloromethyl ketone (ZPCK) were also compared with respect to the known autophagy modulators and were found to be equally effective (Fig. 2B). Validation using the luciferase assay further confirmed the potency of these 2 autophagy inhibitors. The time taken for 50% decay in firefly luciferase activity was found to be significantly reproducible for Bay11 and ZPCK (Fig. 2C and D). These inhibitors also showed a dose-dependent inhibition in autophagy as determined using the luciferase assay (Fig. 2E and F).

The small molecule inhibitors act at different stages of autophagy in yeast Saccharomyces cerevisiae

We performed standard autophagy assays in *S. cerevisiae* for the degradation of autophagy markers, such as the *Saccharomyces cerevisiae* Pot1 (peroxisomal thiolase) tagged with GFP (Pot1-GFP) for pexophagy (Fig. 3A and B) and *Saccharomyces cerevisiae* Atg8, N-terminally tagged with GFP (GFP-Atg8) for general autophagy (Fig. 3E and F). We found that both Bay11 and ZPCK delayed the degradation of peroxisomes, as evident from decreased clearance and consequent slow release of free GFP associated with Pot1-GFP (Fig. 3A–D) and also slower release of GFP in general autophagy assay using GFP-Atg8 as the marker (Fig. 3E–G), which suggests a block in both selective and general autophagy respectively. Fluorescence microscopy studies in *S. cerevisiae* showed a decrease in the degradation of peroxisomes (labeled with Pot1-GFP) in the presence of both the inhibitors as observed by the accumulation of GFP-positive punctate
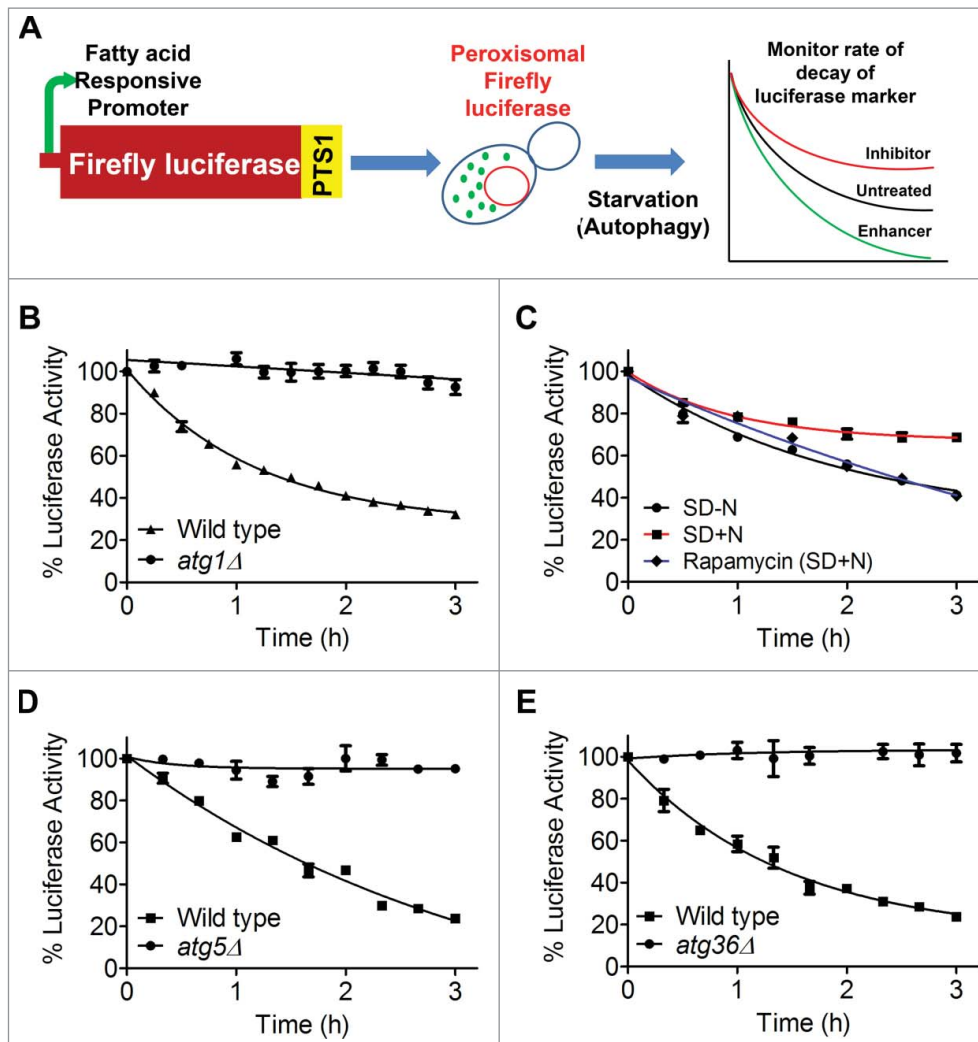
Figure 1. Development of luciferase assay to monitor autophagy in real time. (A) Reporter strain constructed when grown in presence of fatty acid containing media, results in peroxisome biogenesis and drives the expression of firefly luciferase which is targeted to peroxisomes through PTS1 signaling sequence. Once cargo (peroxisome loaded with firefly luciferase) is subjected to starvation, it induces autophagy and results in selective autophagic degradation of peroxisomes (pexophagy). Thus monitoring firefly luciferase activity over time in absence (black line) or in presence of compounds can yield putative inhibitors (red line) or enhancers (green line) of autophagy. (B) The wild-type cells showed a gradual decrease in firefly luciferase counts upon induction of autophagy whereas core autophagy mutant *atg1Δ* showed no drop. (C) Firefly luciferase assay in the presence of starvation (SD-N), nutrient-rich (SD+N) and rapamycin-treated cells. (D) *atg5Δ* and (E) selective autophagy mutant *atg36Δ* (deleted for a receptor protein for pexophagy) did not show any drop in the firefly luciferase activity over time. Z-factor was calculated for 5 assays done in triplicates in 384 well format for firefly luciferase activity. Z-factor for firefly luciferase = 0.8628 ± 0.03481.

structures (peroxisomes or pexophagic bodies) inside or outside of the vacuole (labeled with FM 4–64) (Fig. 3H–L), and lack of diffused GFP signal inside the vacuole (Fig. 3H and K). On the contrary, the number of peroxisomes in the untreated cells decreased in the cytosol with the appearance of diffused GFP inside the vacuole; an indicator of pexophagy (Fig. 3H, K and Vid. S1). However, treatment with 25 μM Bay11 caused the peroxisomes to accumulate outside the vacuoles without any vacuolar diffuse GFP pattern even upon starvation (Fig. 3H, K and Vid. S2). Interestingly, ZPCK (50 μM)-treated cells exhibited a build-up of peroxisomes inside the vacuoles (Fig. 3H, L and Vid. S3). Furthermore, fluorescent microscopy of GFP-labeled autophagosomes (GFP-Atg8) showed accumulation of punctate structures outside the vacuole without any free GFP inside it, on treatment with Bay11 (Fig. 4A–C); a morphology similar to an autophagy mutant (*ypt7Δ*) that blocked the autophagosome-vacuole fusion step. These results indicate that Bay11 likely perturbs at a step before the fusion of autophagosomes with

vacuoles, whereas ZPCK inhibits the degradation of autophagic cargo inside the vacuoles.

To elucidate the step of action of Bay11, a protease protection assay was performed using aminopeptidase as a marker, which is also a substrate for starvation-induced autophagy. Untreated cells in presence of proteinase K showed both the precursor as well as the matured form due to the autophagosome-sequestered membrane-protected cargo and the cytosolic free form, respectively (Fig. 4D and E). However, Bay11-treated cells primarily showed only the mature form of aminopeptidase upon proteinase K treatment (Fig. 4D and E). Combined treatment with proteinase K and triton X-100 resulted in conversion of all the precursor form to the matured form in both treated and untreated groups. Conversion of the precursor to matured form of aminopeptidase in the presence of proteinase K in Bay11-treated cells indicates that the cargo is not protected by the autophagosome membrane, and thus autophagosome biogenesis or maturation or both may be inhibited by Bay11.
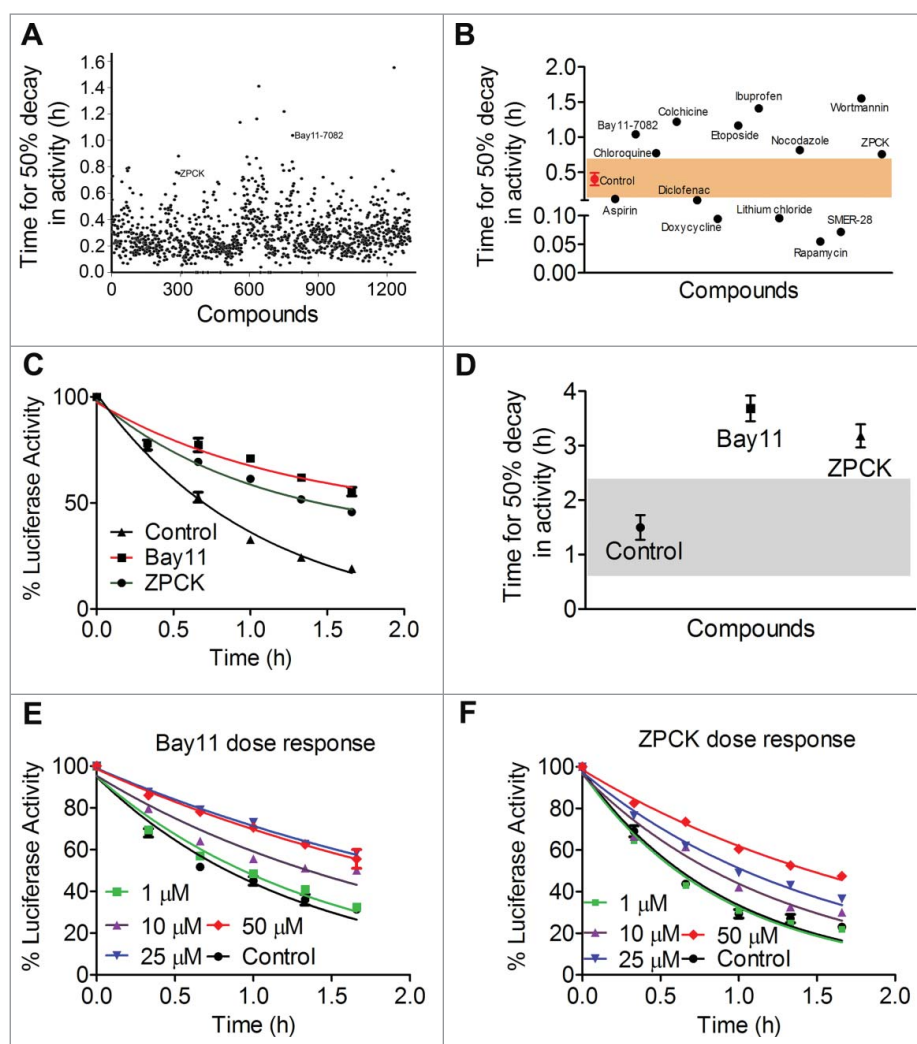
Figure 2. Screening of small molecule libraries. (A) Using the luciferase based assay for monitoring autophagy, the library of pharmacologically active compounds from Sigma containing 1280 FDA-approved small molecules was screened for its effect on autophagy. The rates of degradation of the untreated cells were compared with the ones treated with 50 μM concentration of the compounds. The time taken for 50% decrease in cargo activity (firefly luciferase) was taken as the criteria for comparing the control with the compounds. The compounds that differed from the control by 3 SD units were considered as putative hits. Each black dot represents individual small molecule from the library and the 2 inhibitors Bay11 and ZPCK have also been depicted from the screening data. (B) The dot-plot depicts the comparison between the known modulators picked up from the screen and Bay11 and ZPCK with the shaded region showing the 3 SD area. (C) Two putative inhibitors, Bay11-7082 (Bay11) and Z-L-phenyl chloromethyl ketone (ZPCK) obtained from the primary screening were further confirmed using firefly luciferase assay done in triplicates. (D) Time (in hours) taken for 50% decay in the firefly luciferase activity was plotted for untreated, Bay11- and ZPCK-treated cells (shaded region indicates 3 SD units). (E) A dose-dependent effect on the rates of degradation of firefly luciferase luciferase was seen in Bay11- and (F) ZPCK-treated cells.

Colocalization of Atg8 protein with Atg5, a marker for developing autophagosomes,[33-36] showed only a single Atg5 punctate structure in untreated cells as compared with multiple puncta in Bay11-treated cells (Fig. 4F and G). Also there was significantly more colocalization observed between Atg8 and Atg5 dots in Bay11-treated cells than untreated cells (Fig. 4F and H). This observation taken together with the protease protection assay suggested that the treatment with Bay11 led to accumulation of incompletely formed autophagosomes.

Bay11 and ZPCK inhibit autophagy in mammalian cells

Owing to the conserved nature of autophagy, the putative inhibitors as obtained through the yeast screen were analyzed in mammalian cells for their autophagy inhibitory effects. We assessed the effects of Bay11 and ZPCK in mouse cells for their ability in impairing autophagic cargo degradation by analyzing

the clearance of the specific autophagy substrate, SQSTM1/p62 under basal conditions (nutrient-rich medium).[37] In mouse embryonic fibroblasts (MEFs), we found that both the compounds caused significant accumulation of endogenous SQSTM1 aggregates at 24 h and 48 h (Fig. 5A and B). We further analyzed with Bay11 whether this accumulation of SQSTM1 was autophagy-dependent by using $Atg5^{+/+}$ (wild-type) and $atg5^{-/-}$ (autophagy-deficient) MEFs.[38] As expected, while Bay11 significantly increased endogenous SQSTM1 levels in $Atg5^{+/+}$ MEFs, it had no significant effect in $atg5^{-/-}$ MEFs (Fig. 5C and D). Likewise, Bay11 reduced MAP1LC3B-II levels in $Atg5^{+/+}$ MEFs but not in $atg5^{-/-}$ MEFs that are devoid of autophagosomes or MAP1LC3B-II under basal conditions (Fig. 5E). Densitometric analyses of MAP1LC3B-II:GAPDH and MAP1LC3B-II:MAP1LC3B-I ratios indicate that Bay11 caused a significant reduction of MAP1LC3B-II when analyzed relative to MAP1LC3B-I or GAPDH (Fig. 5F and G).

Table 1. List of hits obtained from screening of LOPAC library

Enhancers (Time taken for 50% decay in luciferase activity in hours)	Inhibitors (Time taken for 50% decay in luciferase activity in hours)
Rapamycin (0.0549)	Ibuprofen (1.409)
Diclofenac (0.1002)	Etoposide (1.164)
Acetohexamide (0.07248)	N-phenylanthranillic acid (0.7936)
Fulvestrant (0.0661)	Cefmetazole sodium (0.7718)
Astaxanthin (0.1027)	Colchicine (1.218)
Fusaric acid (0.05812)	ET-18-OCH3 (0.8643)
GW7647 (0.08532)	Stauroporine aglycone (0.787)
LY-307265 (0.06842)	Gossypol 11 (0.7499)
Indatralin HCl (0.06848)	Cinobufagin (0.8377)
CAPE (0.1223)	Cryptotanshinone (0.7712)
SMER-28 (0.07154)	Methysticin (0.7659)
Grayanotoxin III (0.1272)	Wortmannin (1.551)
Vitexin (0.08347)	Bay11–7082 (1.039)
Doxycycline (0.09441)	ZPCK (0.7575)
Neomycin (0.07297)	Bay11–7085 (0.881)
Aspirin (0.1193)	TNP (0.7888)
Lithium chloride (0.09567)	Chloroquine diphosphate (0.7712)
Retinoic acid (0.0944)	Nocodazole (0.8146)
Nimodipine (0.08418)	
N5-methyl adenosine (0.1047)	
Ritodrine HCl (0.06046)	
AB-MECA (0.1309)	
Esomeprazole Mg dehydrate (0.0679)	
SB242084 dihydrochloride hydrate (0.1085)	
Rottlerin (0.05973)	

Notes. Composite list of all the autophagy modulators (hits) obtained from the screening of the LOPAC library using the luciferase based assay. The screen identified both putative enhancers and inhibitors of autophagy. Numbers in the parenthesis with each compound indicate the time taken for 50% decay in the luciferase activity taken in hours. This was considered as the screening score and compared to only DMSO-treated control, the corresponding screening score was 0.4012 ± 0.08986 h (Mean $\pm$ SD).

To further dissect the step in the autophagy pathway at which the inhibitors act, we performed an autophagosome maturation assay in HeLa cells (immortalized human cervical cancer cells) using tandem-fluorescent-tagged MAP1LC3B reporter, mRFP-GFP-MAP1LC3B.[39] This reporter measures the maturation of autophagosomes into autolysosomes, wherein the autophagosomes emit both mRFP and GFP signals (mRFP$^+$ GFP$^+$) whereas the autolysosomes emit only mRFP signal (mRFP$^+$ GFP$^-$) because GFP is acid-labile and is quenched in the acidic environment. Treatment with 2.5 μM Bay11 decreased the number of autophagosomes (mRFP$^+$ GFP$^+$ puncta) and autolysosomes (mRFP$^+$GFP$^-$ puncta) in HeLa cells expressing mRFP-GFP-MAP1LC3B, whereas treatment with 25 μM ZPCK increased the number of autolysosomes with no significant change in autophagosomes under basal conditions (Fig. 6A and B). Treatment of the inhibitors along with bafilomycin A_1 (BAF), an inhibitor of autophagosome to lysosomal fusion, gave an idea about the inhibition of autophagic flux at different stages. Bay11 blocked at a step before BAF action, whereas ZPCK acted downstream of BAF (Fig. 6A and C). The MAP1LC3B conversion assay was performed under nutrient-rich (Fig. 6D and E), starvation (Fig. 6D and F) and in the presence of BAF (Fig. 6D and G). Relative changes in MAP1LC3B-II:MAP1LC3B-I and MAP1LC3B-II:TUBB ratios were measured. Bay11 decreased the MAP1LC3B-II:MAP1LC3B-I ratio under nutrient-rich and starvation conditions whereas ZPCK increased it in both scenarios (Fig 6D to F). However, although ZPCK showed an increased

MAP1LC3B-II:TUBB ratio, no significant changes were found with Bay11 treatment (Fig 6D–F). Nonetheless, analyzing autophagosome synthesis with BAF revealed that Bay11 reduced the MAP1LC3B-II:TUBB ratio whereas ZPCK had no significant alterations (Fig 6D and G). Moreover, a time-course experiment with prolonged treatment of 12 h under basal conditions with Bay11 resulted in a significant reduction in both MAP1LC3B-II:MAP1LC3B-I (Fig. 6H and I) and MAP1LC3B-II:TUBB (Fig. 6H and J) ratios, further suggesting that Bay11 inhibits autophagosome synthesis. Shorter exposure immunoblots for all the MAP1LC3B conversion assays done for HeLa cells are depicted in Figure S1. Our data suggest that Bay11 inhibited autophagosome biogenesis whereas ZPCK did not affect this event.

To further assess the impact of Bay11 and ZPCK on autophagic degradation in HeLa cells, we analyzed the fluorescence intensity of endogenous SQSTM1 and its colocalization with mRFP-MAP1LC3B-positive autophagosomal compartments. We found that SQSTM1 accumulated either outside or inside the mRFP-MAP1LC3B-positive compartments upon treatment with Bay11 and ZPCK, respectively (Fig. 6K and L). Moreover, the effects of the autophagy blocker BAF were similar to that of ZPCK (Fig. 6K and L). This suggests that Bay11 possibly prevents the loading of SQSTM1 onto autophagosomes or it can inhibit autophagosome biogenesis, leading to lesser availability for SQSTM1 aggregates to colocalize with MAP1LC3B-positive structures. ZPCK like BAF prevents the degradation of SQSTM1 once captured by the autophagosomes, and hence SQSTM1 accumulates in MAP1LC3B-positive structures. This result combined with the data using mRFP-GFP-MAP1LC3B reporter (Fig. 6A) suggests that ZPCK inhibits the degradation of autophagic cargo post autophagosome-lysosome fusion. We next assessed the effects of Bay11 and ZPCK on other trafficking pathways such as endocytosis using the endocytosis-mediated EGFR degradation assay (Fig. 6M). Upon EGF treatment, we found no difference in the degradation of EGFR over time between untreated and treated groups, suggesting that the compounds do not affect general endocytic trafficking (Fig. 6N). Since the EGFR degradation is not affected, which normally occurs in the lysosomal compartments, it is likely that lysosomal proteolytic activity is not perturbed. However, the fact that ZPCK caused accumulation of SQSTM1 suggests that it possibly affects some lysosomal protease specific for autophagic cargo.

Effect of known and novel autophagy modulators on lace plant, Aponogeton madagascariensis: A novel model system to study autophagy in plants

The aquatic lace plant, *Aponogeton madagascariensis*, has leaves that are nearly transparent and ideal for live-cell imaging (Fig. S2A). Leaves taken from axenic cultures were sectioned and then assigned to treatment groups. Treatments included a control with no autophagy modulators (Fig. 7A), overnight starvation (Fig. 7A), 5 μM rapamycin (autophagy enhancer), 5 μM wortmannin (autophagy inhibitor), 1 μM concanamycin A (autophagy inhibitor) (Fig. 7B), 50 μM Bay11 and 50 μM ZPCK (Fig. 7C) and overnight starvation combined with either 5 μM wortmannin, 50 μM Bay11, or 50 μM ZPCK treatments (Fig. 7E). All leaf sections were
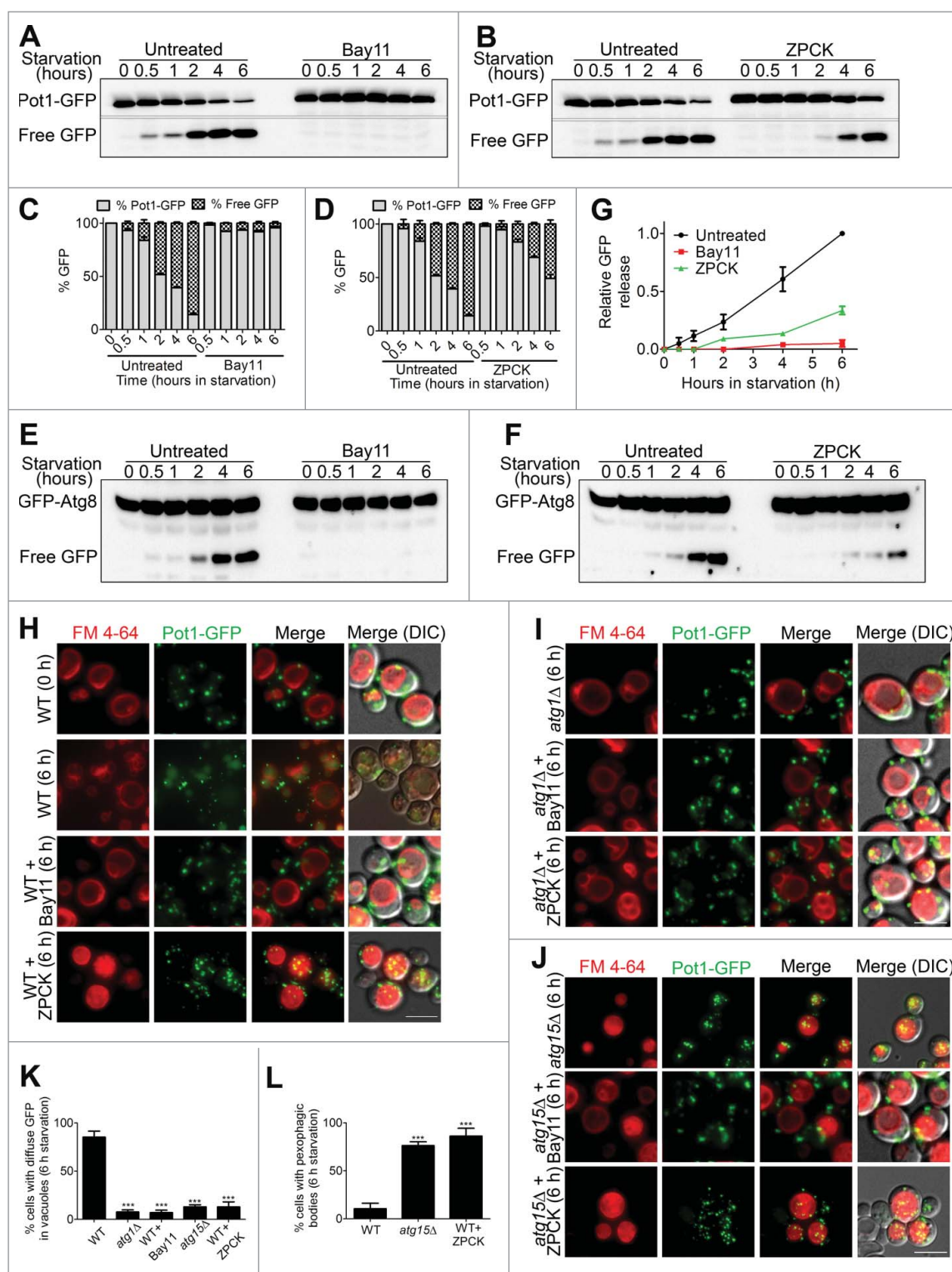
Figure 3. Bay11 blocks the initial step of autophagy whereas ZPCK acts toward the later stages of autophagy in yeast *Saccharomyces cerevisiae*. (A) Pot1-GFP processing assay for assessing the effect of Bay11 and (B) ZPCK on pexophagy. No free GFP release was seen on treatment of wild-type cells with Bay11 even after 6 h of starvation, whereas very little free GFP was observed only at the later time points in ZPCK-treated cells as quantified in (C) and (D). Effect of Bay11 (E) and ZPCK (F) on general auto-phagy was monitored by GFP-Atg8 assay. No or delayed release of GFP was observed on treatment with either Bay11 or ZPCK respectively as compared with the untreated cells (G). Pexophagy (degradation of peroxisomes via autophagy) as monitored via fluorescence microscopy revealed that Bay11 acted at a step before fusion of autophagosomes with the vacuole (H) (labeled with FM 4–64). No free GFP was seen inside the vacuole and the peroxisomes were present in the cytosol even on auto-phagy induction, morphology similar to an early step mutant of autophagy *atg1Δ* (H-J). On treatment with ZPCK, peroxisomes were accumulated inside the vacuole, a morphology similar to *atg15Δ*, an autophagy mutant deficient in a vacuolar lipase (H-J). (K) Quantification showing percentage number of cells with diffuse GFP accumu-lation inside the vacuole in different treatment conditions after 6 h in starvation. (L) Graph showing percentage number of cells with accumulation of pexophagic bodies inside the vacuole on starvation in wild-type, *atg15Δ* and wild-type cells treated with ZPCK.
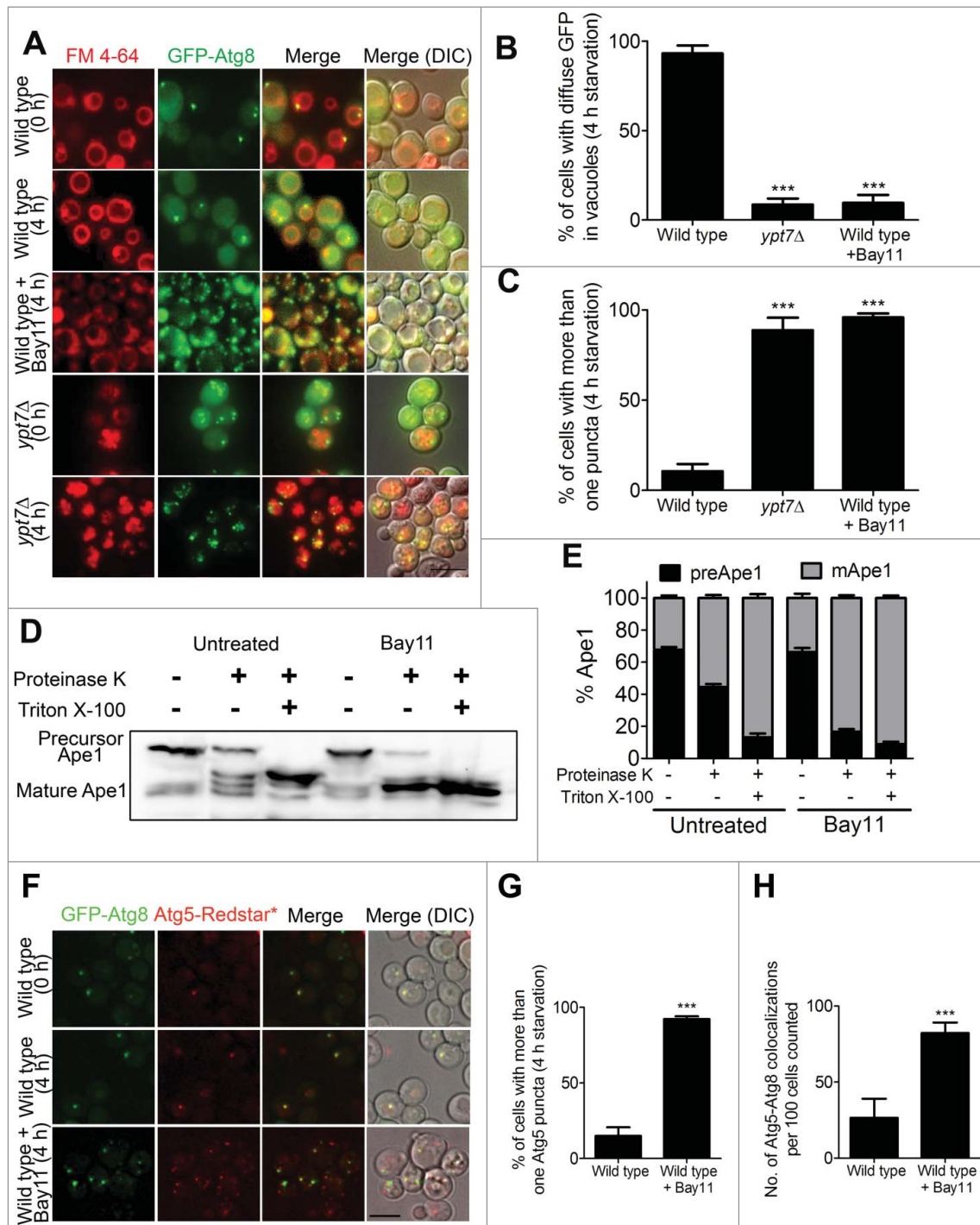
Figure 4. Bay11 treatment affects the maturation of autophagosomes. (A) GFP-Atg8 fluorescence microscopy showed an accumulation of GFP-Atg8-positive puncta on treatment with Bay11 under starvation conditions. Graphs showing diffused GFP inside the vacuole (B) and number of puncta in the cytosol at 4 h of starvation (C) in wild-type, *ypt7Δ* and wild-type cells treated with Bay11. (D) To elucidate the step of action of Bay11, a protease protection assay was performed using aminopeptidase as a marker, which is also a substrate for autophagy on starvation. Conversion of precursor to matured form of aminopeptidase on treatment with proteinase K in Bay11-treated cells indicated that the cargo is not protected by the autophagosome. (E) Quantification showing relative precursor and mature form of aminopeptidase levels for different treatment groups. Y-axis shows the total aminopeptidase levels. (F) Colocalization of genomically tagged GFP-Atg8 and Atg5-RedStar* proteins in untreated and Bay11-treated conditions. (G) Quantification showing percentage number of cells with more than one Atg5 puncta. (H) Quantification showing number of colocalization events per 100 cells in untreated and Bay11-treated cells. Scale bar: 5 μm. Data shown represent a minimum of 100 cells from 3 independent experiments and are expressed as the mean $\pm$ SD. ***$P < 0.001$ (individual means compared using 2-tailed unpaired Student t test).

stained simultaneously with treatment of the modulators using monodansylcadaverine (MDC). The leaf sections were observed using confocal laser scanning microscopy and the mean number of punctate structures per cell were counted for each treatment group and compared with the control, which had a mean of 0.99 $\pm$ 0.12 per cell (Fig. 7D). There were significantly fewer puncta in the wortmannin (0.26 $\pm$ 0.03) (Fig. 7B and D) and Bay11 (0.28 $\pm$ 0.07) (Fig. 7C and D) treatment groups. An overnight starvation for detached leaves resulted in a significant increase in punctate structures (1.90
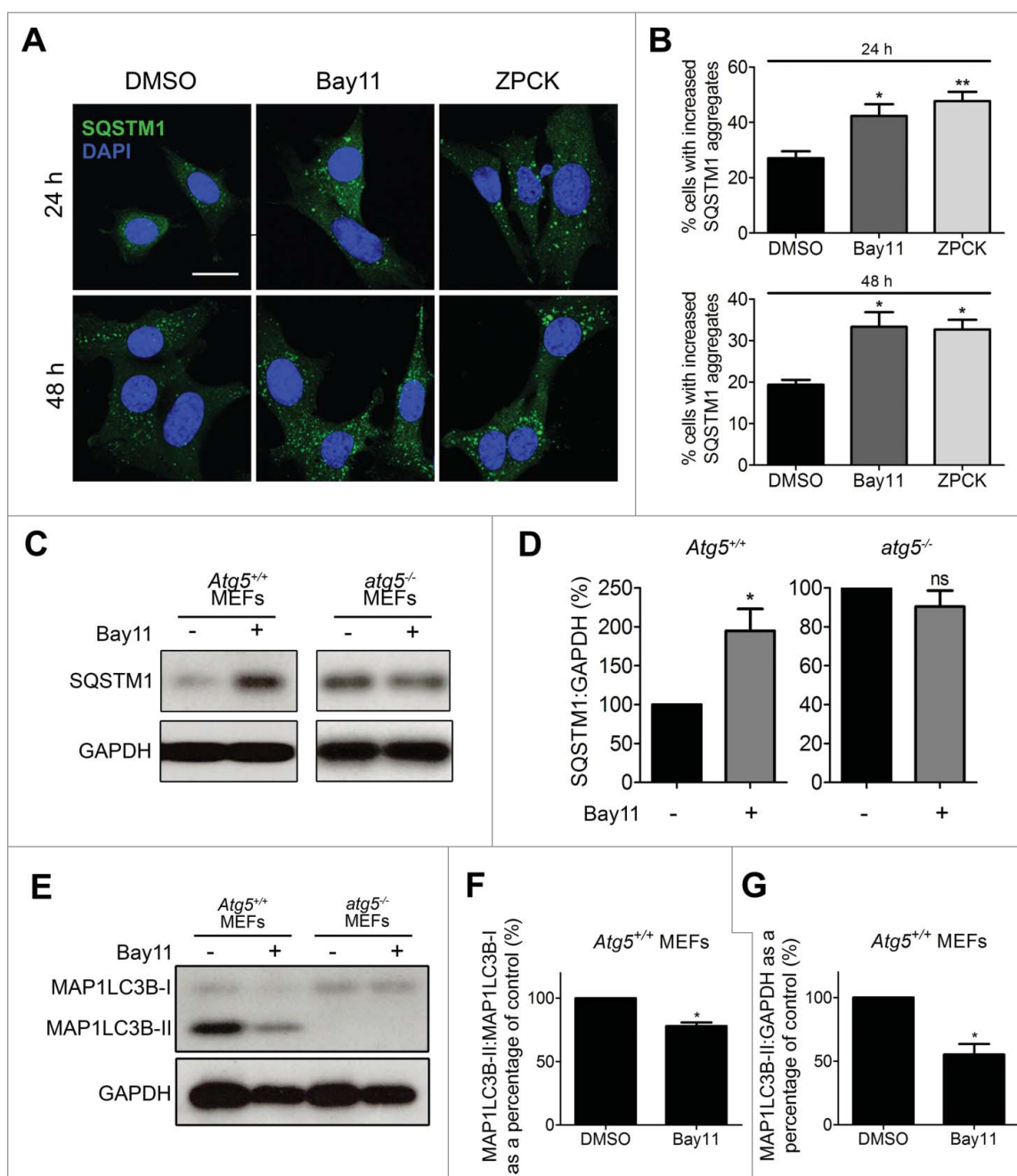
Figure 5. Bay11 and ZPCK inhibit autophagy in MEFs. ((A)and) B) MEFs were treated with DMSO (vehicle control), 5 μM Bay11 or 5 μM ZPCK for 24 h or 48 h under basal conditions, fixed for immunofluorescence analysis with anti-SQSTM1 antibody and imaged by confocal microscopy (A). Analysis was done for the percentage of cells with accumulated endogenous SQSTM1$^+$ aggregates (B). Scale bar: 20 μm. (C and D) $Atg5^{+/+}$ (wild-type) and $atg5^{-/-}$ (autophagy deficient) MEFs were treated with DMSO (vehicle control) or 5 μM Bay11 for 24 h, followed by immunoblotting analysis with anti-SQSTM1 and anti-GAPDH antibodies. Densitometric analysis of SQSTM1 levels was done relative to GAPDH where the control (DMSO-treated) condition was fixed at 100%. (E) $Atg5^{+/+}$ and $atg5^{-/-}$ MEFs were treated with DMSO (vehicle control) or 5 μM Bay11 for 24 h under basal conditions, followed by immunoblotting analysis with anti-MAP1LC3B and anti-GAPDH antibodies. (F) MAP1LC3B-II:MAP1LC3B-I and (G) MAP1LC3B-II:GAPDH levels quantified for 3 independent experiments in DMSO- and Bay11-treated cells.

$\pm$ 0.21) (Fig. 7A, D and E). A significant accumulation of puncta compared with the control was also observed with the concanamycin A (1.91 $\pm$ 0.13) treatment (Fig. 7B and D), but the highest increases in puncta were observed in the rapamycin (2.31 $\pm$ 0.25) (Fig. 7B and D) and ZPCK (3.56 $\pm$ 0.23) treatment groups (Fig. 7C and D). In ZPCK-treated cells the punctate structures appeared to accumulate inside the vacuoles (Vid. S4). Additionally, overnight starvation leaves treated with either Bay11 or wortmannin showed fewer puncta compared with the overnight starvation group, as well as the overnight starvation combined with ZPCK, which had a similar appearance to the starvation group (Fig. 7E).

To confirm that the puncta observed with MDC staining were autophagosomes, immunolocalization experiments were performed using an antibody against Atg8 from *Chlamydomonas reinhardtii* which bears 80% resemblance to *Arabidopsis* Atg8a. The modulators used in MDC experiments were applied to lace plant leaves as mentioned above, the pattern of the punctate structures increased or decreased as expected and was similar to the results obtained from the
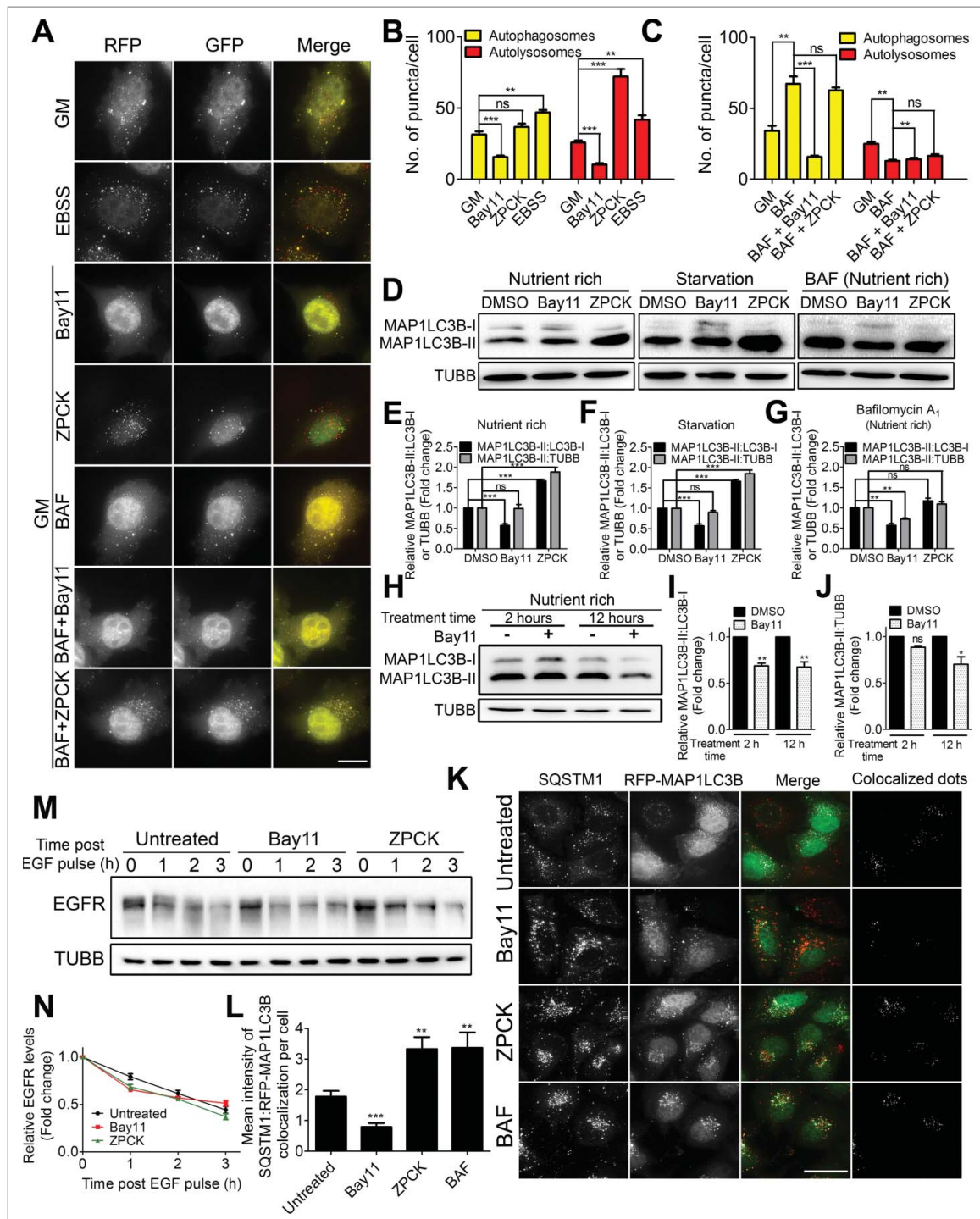
Figure 6. Bay11 and ZPCK inhibit autophagy in HeLa cells at different stages. (A) Hela cells transfected with ptf-MAP1LC3B (vector having tandem mRFP-GFP-tagged MAP1LC3B) treated with either Bay11 or ZPCK for 2 h under basal conditions in the presence or absence of BAF (400 nM) were observed under fluorescence microscope. Autophagosomes appear as yellow dots whereas autolysosomes appear red inside the cells. On treatment with ZPCK, autolysosomes increased inside the cells whereas on Bay11 treatment, very few autophagosomes were seen. Scale bar: 15 μm. (B and C) Data shown represent a minimum of 65 cells from 3 independent experiments with the number of autophagosomes and autolysosomes counted and are expressed as the mean ± SD. ***P < 0.001 (One-way ANOVA, individual means compared with a Dunnett Multiple Comparison Test) (D) MAP1LC3B conversion assay for the mentioned treatment groups under nutrient rich, starvation conditions and along with BAF. ((E)to G) MAP1LC3B-II:MAP1LC3B-I and MAP1LC3B-II:TUBB levels were quantified for all conditions and plotted. (H) MAP1LC3B conversion assay in the absence and presence of Bay11 for 2 and 12 h. (I) MAP1LC3B-II:MAP1LC3B-I and (J) MAP1LC3B-II:TUBB levels of control and Bay11-treated cells over a time course for 3 independent experiments. (K) Immunostaining with SQSTM1 antibody in RFP-MAP1LC3B transfected HeLa cells to assess colocalization. Scale bar: 20 μM (L) Graph showing the amount of colocalization between SQSTM1 and RFP-MAP1LC3B in different treatment groups. The mean intensity of colocalized dots was calculated using the colocalization plug-in of ImageJ analysis software. (M) EGFR trafficking shown by immunoblot for the mentioned treatment groups and degradation levels quantified (N). Data shown represent a minimum of 65 cells from 3 independent experiments and are expressed as the mean ± SD. ***, P < 0.001; **, P < 0.01; *, P < 0.05; ns, nonsignificant (individual means compared by 2-tailed unpaired Student t test).
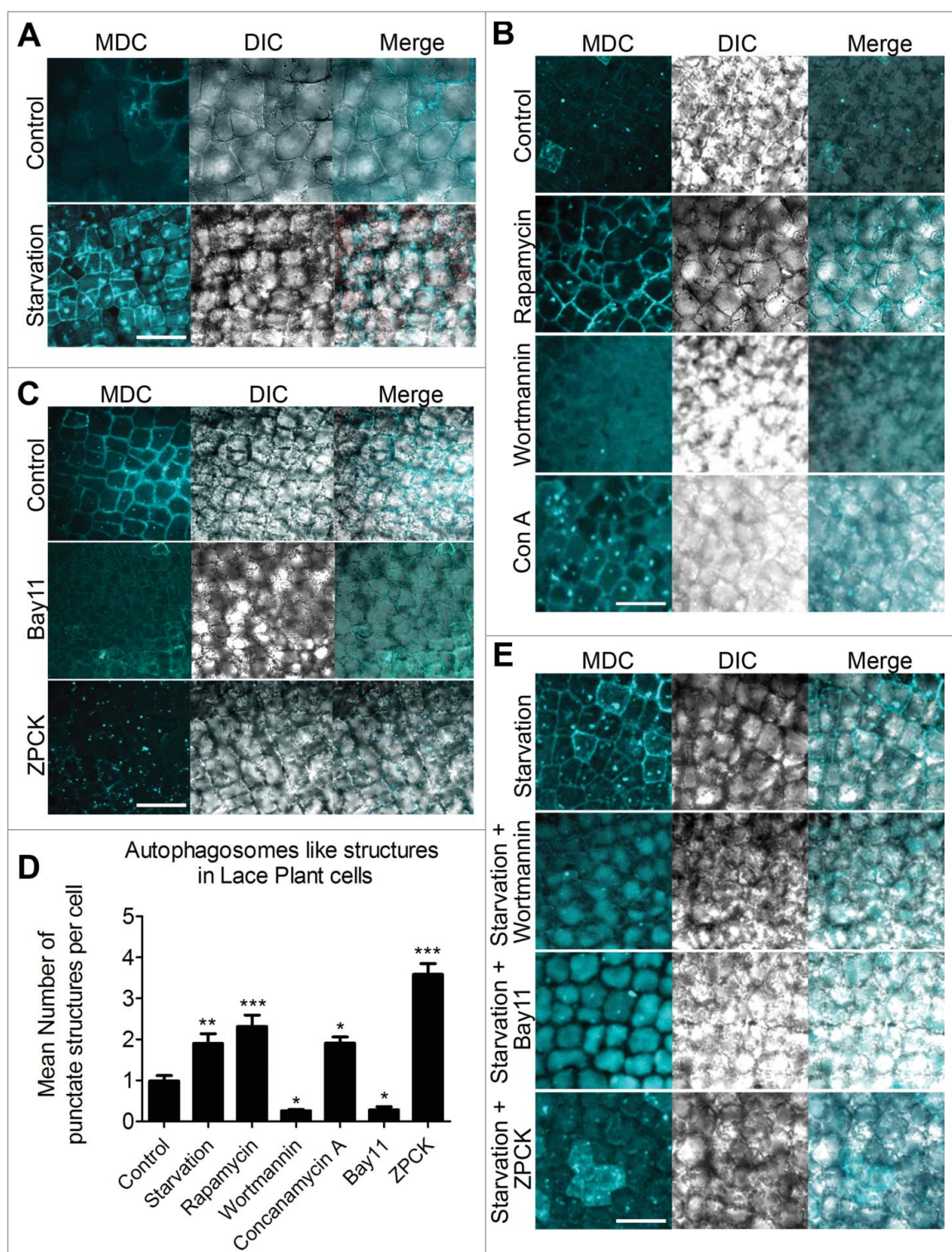
Figure 7. Effect of autophagy modulators in lace plant (*Aponogeton madagascariensis*) cells. Lace plant leaves treated with different modulators were sectioned and stained using monodansylcadaverine (MDC) and scanned via confocal microscopy with 405:450 ± 35nm (ex:em). (A) There were significantly more punctate structures (autophagosome-like structures) in overnight starvation treatment compared with the control. Scale bar: 20 μm (B) The 1 μM concanamycin A and 5 μM rapamycin had a significantly higher number of puncta compared with control, which had more than the 5 μM wortmannin treatment. (C) 50 μM Bay11 significantly reduced, whereas 50 μM ZPCK increased puncta compared with the control. (D) Quantification of the mean number of punctate structures for each treatment (E) Treatment with 50 μM Bay11 or 5 μM wortmannin of overnight starvation leaves showed fewer puncta as compared with the control. Punctate structures were significantly higher than the control in the starvation, and 50 μM ZPCK treatments. Data shown represent a minimum of 4 independent experiments and are expressed as the mean ± SEM. (One-way ANOVA and Dunnett multiple comparison test (***, $P < 0.001$; **, $P < 0.01$; *, $P < 0.05$). Scale bar: 30 μm.

MDC staining procedure (Fig. 8A–C). The control group (Fig. 8A) had 0.90 ± 0.08 puncta (Fig. 8C) and there was a significant inhibition following wortmannin (0.27 ± 0.025; Fig. 8A) and Bay11 (0.22 ± 0.03; Fig. 8B) treatment. There

was a significant increase in puncta following starvation (2.16 ± 0.15; Fig. 8A), rapamycin (3.52 ± 0.09; Fig. 8A), concanamycin A (2.43 ± 0.29; Fig. 8A) and ZPCK (2.09 ± 0.13; Fig. 8B) treatments.
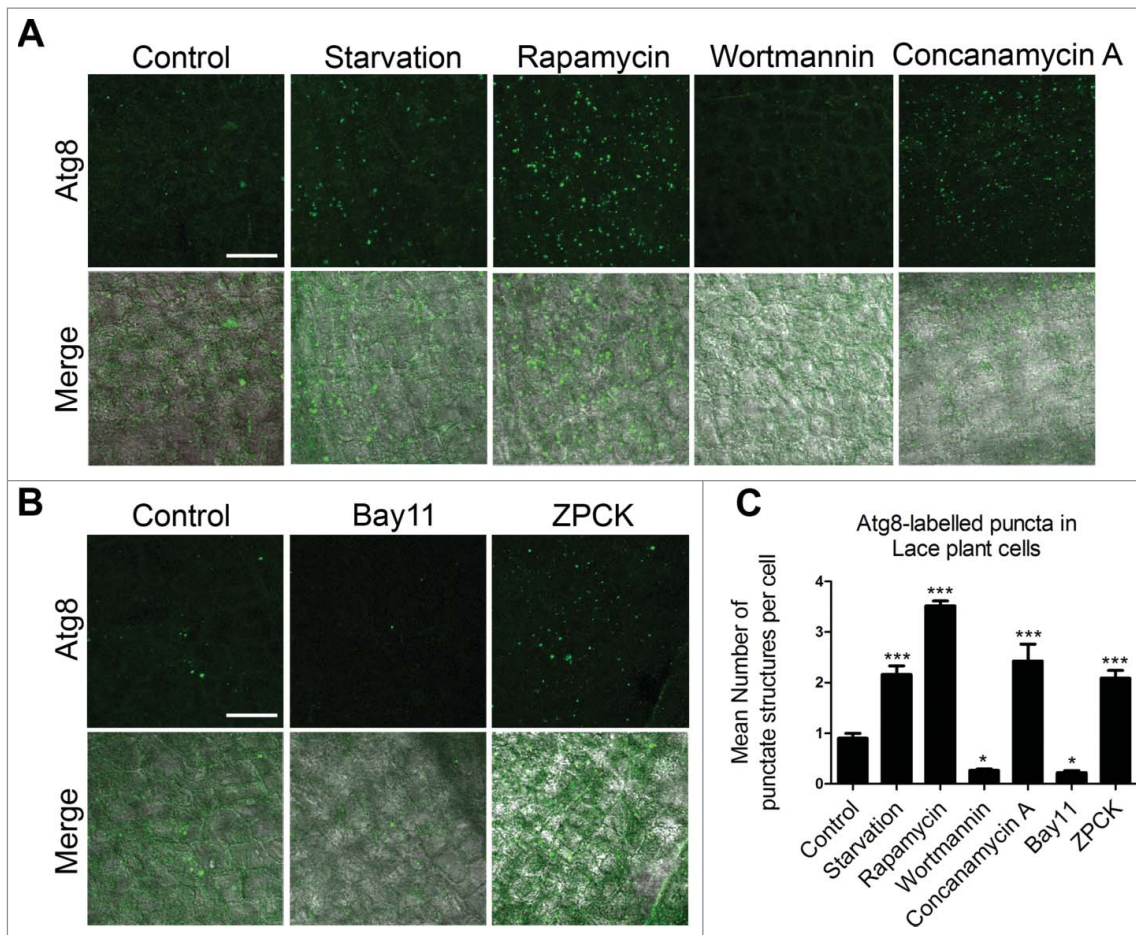
Figure 8. Immunolocalization of Atg8 in lace plant (*Aponogeton madagascariensis*) cells. Lace plant leaf pieces treated with modulators revealed similar results to the MDC staining. (A) The starvation, 5 μM rapamycin and 1 μM concanamycin A treatment groups contained more puncta than the control, while the 5 μM wortmannin treatment reduced puncta. (B) 50 μM Bay 11 reduced the number of puncta and 50 μM ZPCK increased puncta compared with the control group. (C) Quantification was done for a minimum of 4 independent replicates per experimental group and statistical significance was calculated (One-way ANOVA and Dunnett multiple comparison post hoc test ([***], $P < 0.001$; [**], $P < 0.01$; [*], $P < 0.05$). Scale bar: 30 μm.

Discussion

Several studies involving genetic or pharmacological intervention to restore autophagic function in pathophysiological situations such as inflammation, immunity, infection,[14] neurodegeneration,[12, 40] and cancer[41-44] have demonstrated positive outcomes. This has fueled research in identifying novel or repurposed small "drug-like" autophagy modulating molecules that could be of potential therapeutic value.[18, 22, 45] In addition, studies unravelling the mode of action of these molecules provide signaling and mechanistic insights into the regulation of autophagic flux. Key to identifying such important molecules is to have an effective high-throughput assay such as the one described here.

In this study we introduce a luciferase-based assay to monitor autophagy in real time that fulfills several important parameters of an ideal assay, such as high rate of cargo turnover, high sensitivity, robustness and ease of handling. Furthermore, as this assay is not geared toward targeting a specific autophagy-related protein or step in the process, it has the potential to discover small molecules that directly or indirectly modulate different stages of autophagosome biogenesis and turnover. Unlike autophagic flux of cytoplasmic proteins, degradation of an organelle like the peroxisomes is a better alternative to the preexisting assays. Peroxisomes along with

intraorganelle components can be accumulated before their bulk degradation, which occurs in a relatively short period of time involving the core autophagic machinery. This bulk turnover can be monitored by introducing peroxisomally targeted luciferase. These features, when combined with the high sensitivity and vast range of luciferase assays, provide the added benefit of scaling down the assay to a high-throughput level. Z-factor calculated for firefly luciferase activities suggested a very suitable assay which when scaled up to millions of compounds would give fewer false positives and better reliability.

Studies in the past have identified new drug candidates that affect autophagy using yeast or mammalian cells as models. Some of the studies have resulted in drugs of potential clinical utility. Some of these compounds target a particular protein such as ULK1,[46] ATG4[24] or the upstream signaling components such as the class III phosphatidylinositol 3-kinase[47] and MTOR,[48] and target a very specific step in the autophagic flux, whereas other compounds affect autophagy broadly independent of MTOR.[13, 20] In addition, screens performed in the recent past have also identified some compounds with broad spectrum effects as well.[22] While target-driven screens identify molecules that act only at a particular step in autophagy where the target protein is involved, our screen focuses on the entire pathway that can yield hits across all steps of autophagy ranging from upstream

signaling to autophagosome biogenesis-and-maturation to cargo degradation. As a result, using the luciferase assay, we could identify several putative enhancers and inhibitors of autophagic flux even significantly beyond the physiological range of starvation induction. Identification of several known autophagy modulators as hits from the screen further highlighted the strength of the assay. The putative hits from the primary screening of the LOPAC library that includes FDA-approved drugs were further validated. Two of the putative inhibitors identified from the screen, Bay11 and ZPCK, were found to potently affect autophagy using conventional secondary assays. Further investigation to delineate the step of autophagy where the compounds affect showed that they act at distinct stages: Bay11 affected biogenesis or maturation of autophagosomes, whereas ZPCK inhibited the degradation of autophagic bodies and cargo inside the vacuole and lysosomes. Since the assay did not monitor a particular component or target but instead the entire process of autophagy, the effectiveness of the hits in higher eukaryotes was an interesting prospect. Because of the conserved nature of autophagy machinery and the small molecule library comprising of pharmacologically active compounds, it is interesting to see that the autophagy inhibitory effects of the putative hits obtained from our yeast screen are conserved in mammalian and plant cells. We confirmed this not only in well-established mammalian models but also in a novel system such as the lace plant.

For studying autophagy in plants, here we introduced a new model organism, *Aponogeton madagascariensis*, commonly referred to as lace plant, which is a freshwater monocot species found in Madagascar, Comoros, and naturalized in Mauritius.[49] The lace plant is an excellent model system for studying developmentally regulated programmed cell death (PCD) in Plantae (Fig. S2A).[50] The lace plant utilizes PCD to form holes in precise locations during a specific stage in development (Fig. S2B) and ultimately results in perforations by maturity (Fig. S2C). The timing and order of cellular events that occurs during PCD in lace plant leaves is described by Wertman et al.[51] Several types of autophagy have been described in plant cells: microautophagy, macroautophagy and a plant-specific form named mega-autophagy. The role of macroautophagy in the lace plant PCD pathway is not yet understood although mega-autophagy is evident in the later phase of lace plant cell death.[51, 52] Indirect evidence such as increase in vacuolar aggregates (Fig. S2D), vesicle formation (Fig. S2E) and the presence of double-membrane vesicles (Fig. S2F) suggests the involvement of macroautophagy in lace plant cell death.[51, 52] However, whether macroautophagy contributes to the demise of the cell or survival is not yet known.[49] Lace plant is a relatively unexplored system for autophagy; however our data indicate that it is a tractable model system to investigate this phenomenon. When lace plant leaves were treated with several known and novel autophagy modulators, there was a concomitant change in the number of vesicles (MDC staining and Atg8 immunolocalization), further suggesting these vesicles to be autophagosomes. Our results for the overnight starvation, concanamycin A and ZPCK-treated leaves showed a similar staining pattern to concanamycin A-treated *Picea abies* embryo suspensor cells in which mRFP-Atg8 puncta accumulate in the vacuole.[53] Conversely, we showed that wortmannin and Bay11 had fewer puncta, which was similar to wortmannin treated tobacco culture cells stained with quinacrine.[54] The data represented here show that modulators of

autophagy affect vesicular and autophagic flux in lace plants; however their influence on lace plant developmental PCD remains unknown and presents a promising avenue for future research.

From our data (both yeast and mammalian cells), it is evident that Bay11 blocks autophagy at early stages since it reduced MAP1LC3B-positive vesicles at basal state and decreased MAP1LC3B-II levels in BAF-treated cells that consequently led to accumulation of SQSTM1. This suggests that Bay11 inhibits the biogenesis of autophagosomes. However, by analyzing the MAP1LC3B-II:TUBB ratio at the steady-state levels, no decrease by Bay11 was found in HeLa cells unless autophagic flux was clamped with BAF. In addition, we calculated the MAP1LC3B-II:MAP1LC3B-I ratio to account for the accumulation of MAP1LC3B-I levels for an inhibitor like Bay11. We observed a buildup of MAP1LC3B-I levels without any evident change in MAP1LC3B-II, which might suggest a defect in MAP1LC3B lipidation. A time-course experiment with a longer Bay11 treatment resulted in a significant reduction in both MAP1LC3B-II:MAP1LC3B-I and MAP1LC3B-II:TUBB ratios, further indicating the effect of Bay11 on autophagosome synthesis. The data are further corroborated with a decrease in colocalization of MAP1LC3B puncta with SQSTM1, which could be due to ineffective loading of SQSTM1 on autophagosomes and/or decrease in autophagosome availability. Taken together, these results suggest that Bay11 acts at an early stage of autophagosome biogenesis.

Although the autophagosome maturation assay with the mRFP-GFP-MAP1LC3B reporter indicates that ZPCK may act as an autophagy inducer, it also prevents autophagic cargo clearance. ZPCK is a serine protease inhibitor and there are many such proteases that act inside the vacuole to degrade various cargoes. Thus, ZPCK might be acting on some specific proteases responsible for degradation of autophagic cargo in the autolysosomes. These observations are also substantiated by yeast studies where autophagic bodies accumulate inside the vacuole upon ZPCK treatment.

Our data highlights the conserved nature of autophagy that can be used to discover promising novel autophagy regulating small molecules in higher eukaryotes using a yeast-based HTS platform. Further characterization of these small molecules will help in better understanding of the mechanistic insights into the regulation of autophagic flux, and can also help unravel new molecular players in autophagy.

Materials and methods

Yeast strains and plasmids

The wild-type Pot1-GFP strain is a laboratory strain with genomically tagged GFP at the C terminus of Pot1 (HIS selection marker) obtained from Dr. Rachubinski (University of Alberta, Canada) Wild-type BY4741 and all knockout strains were obtained from **EURO**pean *Saccharomyces cerevisiae* **AR**chive for **F**unctional Analysis (EUROSCARF). *S. cerevisiae* shuttle vector pRS306 (URA) was obtained from Prof. Suresh Subramani (UCSD, USA).

Transformation of S. cerevisiae

S. cerevisiae transformation was done using the lithium acetate method. Cells ($\sim$10^8 cells) in early logarithmic phase of growth

were harvested, resuspended in transformation mix (final concentrations: 33.3% PEG 3350 [Sigma-Aldrich, 202444], 0.1 M lithium acetate, 270 μg/ml salmon sperm DNA [Sigma-Aldrich, D1626], 1–1.5 μg DNA) and subjected to heat shock at 42°C for 40 min. Post heat shock cells were harvested and plated onto the selection media plates SD-URA (0.17% yeast nitrogen base [YNB], 0.5% ammonium sulfate, 2% glucose, and amino acids as required without uracil with 2% agar powder) for pRS306P$_{POT1}$-FLUC.

Luciferase assay

The *S. cerevisiae* shuttle vector pRS306 (URA) was used to clone the *Saccharomyces cerevisiae POT1* promoter and the firefly luciferase gene. The oleate responsive region of the *POT1* promoter was amplified from yeast genomic DNA and along with the firefly luciferase gene was cloned into these vectors to obtain the construct pPM3. This plasmid construct was linearized using suitable restriction enzymes in the selection marker and transformed into wild-type and mutant strains of *S. cerevisiae* by standard transformation methods as described above. The colonies were then tested for firefly luciferase activity.

Cells were grown in YPD medium (1% yeast extract, 2% peptone, and 2% glucose) and transferred to oleate medium (0.1% oleic acid [Sigma-Aldrich, 75096], 0.5% Tween-40 [Sigma-Aldrich, P1504], 0.25% yeast extract [Himedia, RM027], 0.5% peptone [Himedia, RM667], 2.64 mM K$_2$HPO$_4$, 17.36 mM KH$_2$PO$_4$, pH 6.0) and incubated overnight at 30°C on a shaker at 250 rpm. Cells were then moved to starvation medium to induce pexophagy [SD-N; 0.17% YNB without ammonium sulfate (Himedia, M151) and 2% dextrose (Himedia, GRM077)]. Samples (A$_{600}$ 3 equivalent) were processed at the mentioned time points using passive lysis buffer (Promega Dual Luciferase Reporter assay system, E1910). Firefly luciferase activity was measured (Spectra max, Molecular devices and Varioskan Flash, Thermo Scientific) after adding the respective substrate in the samples.

Small molecule screening

Small molecule screening was done in the yeast *S. cerevisiae*, where degradation of firefly luciferase was followed over time upon induction of autophagy (Varioskan Flash, Thermo Scientific, USA). Time taken for 50% decrease in cargo activity was plotted for untreated cells and the compounds at 50 μM concentration for the LOPAC compounds. Triplicate values for the control were plotted and a difference of 3 standard deviation (SD) units between the test and control was considered as significant.

Pexophagy assay

Pot1-GFP-positive strains were allowed to grow until the A$_{600}$ reached 0.8–1 in YPD medium. Peroxisome biogenesis was induced by growing these cells in oleate medium for 12 h. Cells were harvested, washed twice to remove traces of oleate and transferred to starvation medium without nitrogen, at inoculum density A$_{600}$ = 3, to induce pexophagy. Cells were collected at various time intervals after pexophagy induction and either

used for microscopy or processed by TCA method as described below for immunoblotting.

GFP-Atg8 processing assay

The *S. cerevisiae* strain containing the GFP-Atg8 (pRS316 vector backbone) plasmid was grown in synthetic defined medium lacking uracil (SD-URA) under appropriate conditions (30°C, 250 rpm). From this, a secondary culture was inoculated at A$_{600}$ = 0.2 and grown as above until A$_{600}$ reached ~0.65. The cultures were transferred to SD-N (nitrogen starvation) medium at A$_{600}$ = 3, separately with and without the compounds, and samples were collected at different time intervals. Collected cells were either used for fluorescence microscopy or sample preparation was done by the TCA precipitation method and immunoblotting was performed as described later.

Atg8 and Atg5 colocalization

For tagging Atg5 with Redstar* fluorescent tag, Redstar* was amplified from pYM42 (EUROSCARF, P30254) plasmid using forward and reverse primers 5′ ACATAACTCTTGTTCCTAT AAAAGGCGGCGATAAAGCTTCCTCTGAGCTCCGTAC GCTGCAGGTCGAC 3′ and 5′ TATTTTCTGCGATATTTG AATGACACTTTTAAATGCGTATATAACAGCTCTTAATC GATGAATTCGAGCTCG 3′ respectively. The PCR product was transformed into *S. cerevisiae* strain containing the GFP-Atg8 (pRS316 vector backbone) plasmid. The dual positive cells (GFP-Atg8 and Atg5 Redstar*) were screened under the microscope.

Yeast cultures were collected at respective time points post treatment, washed and mounted on top of 2% agarose pad and imaged using Delta vision microscope [(API, GE, USA, 29065728), (Olympus 60X/1.42, Plan ApoN, excitation and emission filter FITC and TRITC, polychroic Quad)].

TCA precipitation

All samples were collected in 12.5% TCA final concentration and stored at −80°C for at least half an hour. Later, the samples were thawed on ice and centrifuged for 10 min at 16,000 g and the pellet was washed with 250 μl of ice cold 80% acetone twice and air-dried. This pellet was resuspended in 40 μl of 1% SDS-0.1 N NaOH solution. Sample buffer (5X, 10 μl) was added to the lysate and boiled for 10 min before loading.

Immunoblotting

For HeLa cells, following appropriate treatments, cells were washed with ice cold phosphate-buffered saline (PBS; Sigma, D5773). Cells were then lysed in 100 μl of sample buffer (10% [w:v] SDS, 10 mM DTT, 20% [v:v] glycerol, 0.2 M Tris-HCl, pH 6.8, 0.05% [w:v] bromophenol blue) and then collected using a rubber cell scraper and boiled at 99°C for 15 min.

The HeLa cell lysates and the yeast TCA precipitates were electrophoresed on different percentages of SDS-PAGE based on the desired protein size and transferred onto PVDF membrane at constant current of 2 Ampere for 30 min (Transblot turbo, Bio-Rad Inc., USA). Transfer was confirmed by Ponceau

S staining of blots. Blots were incubated overnight with 5% skim milk in primary antibody (anti-GFP: Roche, 11814460001; anti-MAP1LC3B: Cell Signaling Technology, L7543). Secondary antibody used at 1:10,000 was goat anti-mouse (Bio-Rad, 172–1011) or goat anti-rabbit antibody conjugated to HRP (Bio-Rad, 172–1019). Blots were developed by using ECL substrate (Thermo Scientific, 34087 or Bio-Rad, 170–5061) and images captured using an auto capture program in Syngene G-Box, UK. ImageJ (NIH) was used for quantification of band intensities.

Immunoblotting in MEFs was performed as described previously.[22] Dilutions of primary antibodies used were as follows: Anti-SQSTM1/p62 1:1000 (Progen Biotechnik, GP62-C), anti-MAP1LC3B 1:3000 (Novus Biologicals, NB100–2220) and anti-GAPDH (Cell Signaling Technologies, 2118S). Secondary antibodies conjugated to HRP were used at 1:10000 dilution as follows: Anti-guinea pig-HRP (Abcam, ab50210) and anti-rabbit-HRP (Calbiochem, 401393).

Culturing of cells

HeLa cells were maintained in growth medium comprised of Dulbecco's modified Eagle's medium (DMEM; Sigma-Aldrich, D5648) supplemented with 3.7 g/L sodium bicarbonate plus 10% fetal bovine serum (FBS; PAN, 3302-P121508) and 100 units/ml of penicillin and streptomycin (Sigma-Aldrich, P4333) at 5% CO_2 and 37°C. $Atg5^{+/+}$ and $atg5^{-/-}$ MEFs[38] were cultured in DMEM (ThermoFisher Scientific, 41965–039) supplemented with 10% FBS (ThermoFisher Scientific, 10270–106), 100 units/ml of penicillin and streptomycin (ThermoFisher Scientific, 15070–063) and 2 mM L-glutamine (ThermoFisher Scientific, 25030–024) at 37°C in a humidified incubator under 5% CO_2.

Immunofluorescence

An appropriate number of cells was plated on top of coverslips placed in 65-mm cell culture dishes for transfection. Transfected cells were divided into different treatment groups. Post treatment, cells were washed with phosphate-buffered saline and fixed in 4% paraformaldehyde and permeabilized using 0.25% Triton X-100 (Himedia, MB031). Overnight incubation with anti-SQSTM1/p62 (rabbit polyclonal; MBL, PM045), and anti-EEA1 (rabbit polyclonal; Cell Signaling Technology, 3288) was done at 4°C. Excess antibody was washed with PBS and coverslips were incubated with Atto-633 (goat anti-rabbit IgG; Sigma, 41176). The coverslips were mounted with VECTA-SHIELD antifade reagent (Vector laboratories, H-1000/H-1200). Imaging for HeLa cells was performed using a Delta vision microscope [(API, GE, USA, 29065728), (Olympus 60X/1.42, Plan ApoN, excitation and emission filter Cy5, FITC and TRITC, polychroic Quad)].

Immunofluorescence analysis in MEFs was performed by fixing the cells with 4% methanol-free paraformaldehyde for 15 min, permeabilized with 0.5% TritonX-100 in PBS for 10 min, and then blocking with 5% FBS in PBS for 30 min at room temperature, along with PBS washes in between every steps. An anti-SQSTM1 antibody (Progen Biotechnik, GP62-C) was used at 1:250 dilution in 5% FBS in PBS and incubated overnight at 4°C. Cells were then washed and incubated with goat anti-guinea pig Alexa Fluor 594 (ThermoFisher Scientific, A-11076) secondary antibody at 1:1000 dilution for 1 h at room temperature. Cells were washed, counterstained with DAPI (ThermoFisher Scientific, D1306) in PBS for 5 min, washed again and then mounted using Prolong diamond anti-fade reagent (ThermoFisher Scientific, P36970). Slides were imaged using a Zeiss LSM 510 Meta Confocal Microscope (Carl Zeiss, Germany) using a 100X objective. Analysis was performed by assessing for the percentage of cells displaying an accumulation of endogenous SQSTM1-positive aggregates.

Analysis of autophagosome maturation using mRFP-GFP-MAP1LC3B reporter

Transfection was done on a 60-mm dish with HeLa cells at 60 to 70% confluency. Cells were transfected with tandem RFP-GFP-MAP1LC3B construct (Addgene, 21074, deposited by Tamotsu Yoshimori) using 5 μl of Lipofectamine 2000 (Invitrogen, 11668–019) and 2.5 μg of DNA (2:1 ratio) diluted in 100 μl of OPTI-MEM (Invitrogen, 31985–070) separately. Seventy-two h after transfection, cells were either left untreated or treatment with various concentrations of Bay11–7082 (Sigma-Aldrich, B5556) or ZPCK (Sigma-Aldrich, 860794) was done for 2 h. Starvation was induced by treating cells with Earle balanced salt solution. After treatment, cells were fixed in 4% paraformaldehyde and permeabilized using 0.25% Triton X-100. The coverslip was mounted with VECTASHIELD antifade reagent. Imaging for HeLa cells was performed using a Delta vision microscope (Olympus 60X/1.42, Plan ApoN, excitation and emission filter, FITC and TRITC, polychroic Quad).

EGFR trafficking

HeLa cells were plated on 6-well plates and allowed to attach on the surface. The cells were washed with PBS and then starved in DMEM (serum-free medium) for 3 h. Pretreatment with compounds was performed for 1 h, following which they were pulsed with 100 ng/ml of EGF (Life Technologies, PHG0311L) and samples were collected at 0, 1, 2 and 3 h.

Quantification of cells with increased SQSTM1$^+$ aggregates

Analysis of SQSTM1 aggregates was done as described previously.[55] Briefly, immunofluorescence analysis with anti-SQSTM1 antibody was performed for assessing endogenous SQSTM1$^+$ aggregates using confocal microscopy. The percentage of cells with increased SQSTM1$^+$ aggregates was quantified by assessing 200 cells per condition from independent experiments, in which a cell with an accumulation of SQSTM1$^+$ aggregates was given a score of 1 whereas a cell having basal (low) levels of SQSTM1$^+$ aggregates was given a score of 0.

Mean intensity calculation

ImageJ software (NIH) was used to calculate the mean intensity. Images were opened using the split channel plugin. The

colocalization plugin in the analysis tools was used to obtain the colocalized area between 2 channels as a separate window. The intensity was calculated using the measure plugin in analysis tools.

Lace plant cultures and experiments

Axenic lace plant cultures were grown in magenta boxes (Fig. S2A) and prepared according to Gunawardena et al.[56] Leaves in the window stage were removed from the corm and rinsed thoroughly with distilled water before being sectioned into 2-mm^2 pieces. For starvation treatments, window stage leaves were removed from the plant, placed in distilled water and kept in the dark overnight. Leaf sections were stained with monodansylcadaverine (300 μM; Sigma, D4008) and simultaneously treated with autophagy modulators for 2 h in the dark (1 h vacuum infiltration at 15 psi). Treatment times, along with stain and modulator applications were optimized using concentration gradients followed by microscopy. The optimized concentrations were 5 μM rapamycin (Enzo Life Sciences [BML-A275–0005], 5 μM wortmannin [Santa Cruz Biotechnology, sc-3505], 1 μM concanamycin A [Santa Cruz Biotechnology, sc-202111], 50 μM Bay11 and 50 μM ZPCK. Tissue sections were then rinsed and mounted in distilled water before being scanned using a Nikon Eclipse Ti confocal microscope [(Nikon Canada, Mississauga, ON) (Nikon 40X/1.30, Plan Fluor, 405 nm excitation and 450/30 nm emission)]. Areoles in the early phases of PCD were scanned to avoid cellular debris. The mean number of puncta were quantified for each treatment group with a minimum of 4 independent experiments using NIS Elements Advanced Research software. Additionally, starvation treatment leaves were also exposed to 5 μM wortmannin, 50 μM Bay11 and 50 μM ZPCK treatments and then qualitatively accessed via confocal microscopy.

Immunostaining in lace plant

Atg8 immunolocalization in lace plant window stage leaves was achieved using a modified protocol from Pasternak et al.[57] Whole leaves were treated for 2 h before fixation in 100% methanol at 37°C and then hydrophilized to 20% methanol by adding distilled water at 60°C every 2 min for 32 min. Samples were then sectioned and placed on a multi-wall slide and allowed to air dry for 10 min to facilitate membrane permeabilization. Blocking was done for 30 min at 37°C with 4% lowfat milk powder in 1X microtubule stabilization buffer MTSB (modified 2X MTSB stock solution: 15 g PIPES (Bioshop Canada, PIP666), 1.9 g EDTA, 1.22 g MgSO$_4$*7H$_2$O, 2.5 g KOH, pH 7.0). Regarding Atg8, the primary antibody incubation for anti-*Chlamydomonas reinhardtii* Atg8 (Agrisera, AS14 2769), produced in rabbit, was done at a 1:1000 dilution in 1X MTSB for 30 min at 37°C. Samples were then washed for 5 min, 3 times with 1X MTSB. Secondary antibody incubation with goat anti-rabbit Dylight 488 (Agrisera, AS09 633) at a 1:2000 dilution in 1X MTSB was done for 30 min at 37°C and then samples were rinsed as above. Tissues were mounted in Mowiol 4–88 solution (Sigma, 81381) and scanned via confocal microscopy as mentioned above. The mean number of puncta per cell was determined using maximum intensity projections (MIPs) for each replicate. The total number of cells within a field of view were counted manually and the number of puncta were counted automatically using ImageJ.

Statistical analysis and image preparation

Statistical analysis was performed using GraphPad Prism (GraphPad Sofware). Statistical analyses were performed by comparing the means using the unpaired Student t test and one-way ANOVA followed by the Dunnett multiple comparision post-hoc test. Yeast and mammalian images were prepared using Softworx software (GE healthare). Lace plant MIP images were prepared using NIS elements software (Nikon, Canada). Images were plated using Adobe Photoshop CC. Fluorescent MIP images had their brightness and contrast modified equally using Adobe Photoshop CC.

Abbreviations

A$_{600}$	absorbance at 600 nmApe1 aminopeptidase
FDA	food and drug administration
GFP	green fluorescent protein
GM	growth medium
HTS	high-throughput screen
IBAF	bafilomycin A$_1$
LOPAC	library of pharmacologically active compounds
MEF	mouse embryonic fibroblast
MIPs	maximum intensity projections
PBS	phosphate-buffered saline
PCD	programmed cell deathPot1 peroxisomal thiolase
PTS1	peroxisomal targeting signal 1RFP red fluorescent protein
SD	standard deviation
SEM	standard error mean ZPCK Z-L-phenyl chloromethyl ketone

Disclosure of potential conflicts of interest

The authors declare that they have no potential conflict of interest.

References

[1] Meijer WH, van der Klei IJ, Veenhuis M, Kiel JA. ATG genes involved in non-selective autophagy are conserved from yeast to man, but the selective Cvt and pexophagy pathways also require organism-specific genes. Autophagy 2007; 3:106-16; PMID:17204848; https://doi.org/10.4161/auto.3595

[2] Boya P, Reggiori F, Codogno P. Emerging regulation and functions of autophagy. Nat Cell Biol 2013; 15:713-20; PMID:23817233; https://doi.org/10.1038/ncb2788

[3] Rabinowitz JD, White E. Autophagy and metabolism. Science 2010; 330:1344-8; PMID:21127245; https://doi.org/10.1126/science.1193497

[4] Klionsky DJ. Autophagy: from phenomenology to molecular understanding in less than a decade. Nat Rev Mol Cell Biol 2007; 8:931-7; PMID:17712358; https://doi.org/10.1038/nrm2245

[5] Komatsu M, Ichimura Y. Selective autophagy regulates various cellular functions. Genes Cells 2010; 15:923-33; https://doi.org/10.1111/j.1365-2443.2010.01433.x

[6] Mizushima N, Klionsky DJ. Protein turnover via autophagy: implications for metabolism. Annual Rev Nutri 2007; 27:19-40; PMID:17311494; https://doi.org/10.1146/annurev.nutr.27.061406.093749

[7] Musiwaro P, Smith M, Manifava M, Walker SA, Ktistakis NT. Characteristics and requirements of basal autophagy in HEK 293 cells. Autophagy 2013; 9:1407-17; PMID:23800949; https://doi.org/10.4161/auto.25455

[8] Kroemer G. Autophagy: a druggable process that is deregulated in aging and human disease. J Clin Invest 2015; 125:1-4; PMID:25654544; https://doi.org/10.1172/JCI78652

[9] White E, DiPaola RS. The double-edged sword of autophagy modulation in cancer. Clin Cancer Res 2009; 15:5308-16; PMID:19706824; https://doi.org/10.1158/1078-0432.CCR-07-5023

[10] White E. Deconvoluting the context-dependent role for autophagy in cancer. Nat Rev Cancer 2012; 12:401-10; PMID:22534666; https://doi.org/10.1038/nrc3262

[11] Son JH, Shim JH, Kim KH, Ha JY, Han JY. Neuronal autophagy and neurodegenerative diseases. Exp Mol Med 2012; 44:89-98; https://doi.org/10.3858/emm.2012.44.2.031

[12] Nixon RA. The role of autophagy in neurodegenerative disease. Nat Med 2013; 19:983-97; PMID:23921753; https://doi.org/10.1038/nm.3232

[13] Rubinsztein DC, Codogno P, Levine B. Autophagy modulation as a potential therapeutic target for diverse diseases. Nat Rev Drug Discovery 2012; 11:709-30; PMID:22935804; https://doi.org/10.1038/nrd3802

[14] Gutierrez MG, Master SS, Singh SB, Taylor GA, Colombo MI, Deretic V. Autophagy is a defense mechanism inhibiting BCG and Mycobacterium tuberculosis survival in infected macrophages. Cell 2004; 119:753-66; PMID:15607973; https://doi.org/10.1016/j.cell.2004.11.038

[15] Wild P, Farhan H, McEwan DG, Wagner S, Rogov VV, Brady NR, Richter B, Korac J, Waidmann O, Choudhary C, et al. Phosphorylation of the autophagy receptor optineurin restricts Salmonella growth. Science 2011; 333:228-33; PMID:21617041; https://doi.org/10.1126/science.1205405

[16] Ogawa M, Yoshimori T, Suzuki T, Sagara H, Mizushima N, Sasakawa C. Escape of intracellular Shigella from autophagy. Science 2005; 307:727-31; PMID:15576571; https://doi.org/10.1126/science.1106036

[17] Nakagawa I, Amano A, Mizushima N, Yamamoto A, Yamaguchi H, Kamimoto T, Nara A, Funao J, Nakata M, Tsuda K, et al. Autophagy defends cells against invading group A Streptococcus. Science 2004; 306:1037-40; PMID:15528445; https://doi.org/10.1126/science.1103966

[18] Sarkar S, Rubinsztein DC. Small molecule enhancers of autophagy for neurodegenerative diseases. Mol Bio Systems 2008; 4:895-901

[19] Ravikumar B, Vacher C, Berger Z, Davies JE, Luo S, Oroz LG, Scaravilli F, Easton DF, Duden R, O'Kane CJ, et al. Inhibition of mTOR induces autophagy and reduces toxicity of polyglutamine expansions in fly and mouse models of Huntington disease. Nat Genetics 2004; 36:585-95; PMID:15146184; https://doi.org/10.1038/ng1362

[20] Sarkar S. Regulation of autophagy by mTOR-dependent and mTOR-independent pathways: autophagy dysfunction in neurodegenerative diseases and therapeutic application of autophagy enhancers. Biochem Soc Transactions 2013; 41:1103-30; PMID:24059496; https://doi.org/10.1042/BST20130134

[21] Chauhan S, Ahmed Z, Bradfute SB, Arko-Mensah J, Mandell MA, Won Choi S, Kimura T, Blanchet F, Waller A, Mudd MH, et al. Pharmacological screen identifies novel target processes for activation of autophagy with a broad translational potential. Nat Commun 2015; 6:8620; PMID:26503418; https://doi.org/10.1038/ncomms9620

[22] Sarkar S, Perlstein EO, Imarisio S, Pineau S, Cordenier A, Maglathlin RL, Webster JA, Lewis TA, O'Kane CJ, Schreiber SL, et al. Small molecules enhance autophagy and reduce toxicity in Huntington's disease models. Nat Chem Biol 2007; 3:331-8; PMID:17486044; https://doi.org/10.1038/nchembio883

[23] Ju JS, Miller SE, Jackson E, Cadwell K, Piwnica-Worms D, Weihl CC. Quantitation of selective autophagic protein aggregate degradation in vitro and in vivo using luciferase reporters. Autophagy 2009; 5:511-9; PMID:19305149; https://doi.org/10.4161/auto.5.4.7761

[24] Ketteler R, Seed B. Quantitation of autophagy by luciferase release assay. Autophagy 2008; 4:801-6; PMID:18641457; https://doi.org/10.4161/auto.6401

[25] Klionsky DJ, Abdelmohsen K, Abe A, Abedin MJ, Abeliovich H, Acevedo Arozena A, Adachi H, Adams CM, Adams PD, Adeli K, et al. Guidelines for the use and interpretation of assays for monitoring autophagy (3rd edition). Autophagy 2016; 12:1-222; PMID:26799652; https://doi.org/10.1080/15548627.2015.1100356

[26] Sarkar S. Chemical screening platforms for autophagy drug discovery to identify therapeutic candidates for Huntington's disease and other neurodegenerative disorders. Drug Discovery Today Technologies 2013; 10:e137-44; PMID:24050242; https://doi.org/10.1016/j.ddtec.2012.09.010

[27] Sakai Y, Oku M, van der Klei IJ, Kiel JA. Pexophagy: autophagic degradation of peroxisomes. Biochim Et Biophys Acta 2006; 1763:1767-75; PMID:17005271; https://doi.org/10.1016/j.bbamcr.2006.08.023

[28] Dunn WA, Jr, Cregg JM, Kiel JA, van der Klei IJ, Oku M, Sakai Y, Sibirny AA, Stasyk OV, Veenhuis M. Pexophagy: the selective autophagy of peroxisomes. Autophagy 2005; 1:75-83; PMID:16874024; https://doi.org/10.4161/auto.1.2.1737

[29] Farre JC, Manjithaya R, Mathewson RD, Subramani S. PpAtg30 tags peroxisomes for turnover by selective autophagy. Dev Cell 2008; 14:365-76; PMID:18331717; https://doi.org/10.1016/j.devcel.2007.12.011

[30] Manjithaya R, Jain S, Farre JC, Subramani S. A yeast MAPK cascade regulates pexophagy but not other autophagy pathways. J Cell Biol 2010; 189:303-10; PMID:20385774; https://doi.org/10.1083/jcb.200909154

[31] Ma C, Schumann U, Rayapuram N, Subramani S. The peroxisomal matrix import of Pex8p requires only PTS receptors and Pex14p. Mol Biol Cell 2009; 20:3680-9; PMID:19570913; https://doi.org/10.1091/mbc.E09-01-0037

[32] Mathieu M, Modis Y, Zeelen JP, Engel CK, Abagyan RA, Ahlberg A, Rasmussen B, Lamzin VS, Kunau WH, Wierenga RK. The 1.8 A crystal structure of the dimeric peroxisomal 3-ketoacyl-CoA thiolase of Saccharomyces cerevisiae: implications for substrate binding and reaction mechanism. J Mol Biol 1997; 273:714-28; PMID:9402066; https://doi.org/10.1006/jmbi.1997.1331

[33] Suzuki K, Kubota Y, Sekito T, Ohsumi Y. Hierarchy of Atg proteins in pre-autophagosomal structure organization. Genes Cells 2007; 12:209-18; https://doi.org/10.1111/j.1365-2443.2007.01050.x

[34] Suzuki K, Akioka M, Kondo-Kakuta C, Yamamoto H, Ohsumi Y. Fine mapping of autophagy-related proteins during autophagosome formation in Saccharomyces cerevisiae. J Cell Sci 2013; 126:2534-44; PMID:23549786; https://doi.org/10.1242/jcs.122960

[35] Graef M, Friedman JR, Graham C, Babu M, Nunnari J. ER exit sites are physical and functional core autophagosome biogenesis components. Mol Biol Cell 2013; 24:2918-31; PMID:23904270; https://doi.org/10.1091/mbc.E13-07-0381

[36] Romanov J, Walczak M, Ibiricu I, Schuchner S, Ogris E, Kraft C, Martens S. Mechanism and functions of membrane binding by the

Atg5-Atg12/Atg16 complex during autophagosome formation. EMBO J 2012; 31:4304-17; PMID:23064152; https://doi.org/10.1038/emboj.2012.278

[37] Bjorkoy G, Lamark T, Brech A, Outzen H, Perander M, Overvatn A, Stenmark H, Johansen T. p62/SQSTM1 forms protein aggregates degraded by autophagy and has a protective effect on huntingtin-induced cell death. J Cell Biol 2005; 171:603-14; PMID:16286508; https://doi.org/10.1083/jcb.200507002

[38] Kuma A, Hatano M, Matsui M, Yamamoto A, Nakaya H, Yoshimori T, Ohsumi Y, Tokuhisa T, Mizushima N. The role of autophagy during the early neonatal starvation period. Nature 2004; 432:1032-6; PMID:15525940; https://doi.org/10.1038/nature03029

[39] Kimura S, Noda T, Yoshimori T. Dissection of the autophagosome maturation process by a novel reporter protein, tandem fluorescent-tagged LC3. Autophagy 2007; 3:452-60; PMID:17534139; https://doi.org/10.4161/auto.4451

[40] Ravikumar B, Duden R, Rubinsztein DC. Aggregate-prone proteins with polyglutamine and polyalanine expansions are degraded by autophagy. Hum Mol Genetics 2002; 11:1107-17; PMID:11978769; https://doi.org/10.1093/hmg/11.9.1107

[41] Liang XH, Jackson S, Seaman M, Brown K, Kempkes B, Hibshoosh H, Levine B. Induction of autophagy and inhibition of tumorigenesis by beclin 1. Nature 1999; 402:672-6; PMID:10604474; https://doi.org/10.1038/45257

[42] Kuo SY, Castoreno AB, Aldrich LN, Lassen KG, Goel G, Dancik V, Kuballa P, Latorre I, Conway KL, Sarkar S, et al. Small-molecule enhancers of autophagy modulate cellular disease phenotypes suggested by human genetics. Proc Natl Acad Sci U S A 2015; 112:E4281-7; PMID:26195741; https://doi.org/10.1073/pnas.1512289112

[43] Mathew R, Karantza-Wadsworth V, White E. Role of autophagy in cancer. Nat Rev Cancer 2007; 7:961-7; PMID:17972889; https://doi.org/10.1038/nrc2254

[44] Qu X, Yu J, Bhagat G, Furuya N, Hibshoosh H, Troxel A, Rosen J, Eskelinen EL, Mizushima N, Ohsumi Y, et al. Promotion of tumorigenesis by heterozygous disruption of the beclin 1 autophagy gene. J Clin Invest 2003; 112:1809-20; PMID:14638851; https://doi.org/10.1172/JCI20039

[45] Egan DF, Chun MG, Vamos M, Zou H, Rong J, Miller CJ, Lou HJ, Raveendra-Panickar D, Yang CC, Sheffler DJ, et al. Small Molecule Inhibition of the Autophagy Kinase ULK1 and Identification of ULK1 Substrates. Mol Cell 2015; 59:285-97; PMID:26118643; https://doi.org/10.1016/j.molcel.2015.05.031

[46] Rosenberg LH, Lafitte M, Grant W, Chen W, Cleveland JL, Duckett DR. Development of an HTS-compatible assay for the discovery of Ulk1 inhibitors. J Biomol Screening 2015; 20:913-20; PMID:25851035; https://doi.org/10.1177/1087057115579391

[47] Farkas T, Daugaard M, Jaattela M. Identification of small molecule inhibitors of phosphatidylinositol 3-kinase and autophagy. J Biol Chem 2011; 286:38904-12; PMID:21930714; https://doi.org/10.1074/jbc.M111.269134

[48] Butcher RA, Bhullar BS, Perlstein EO, Marsischky G, LaBaer J, Schreiber SL. Microarray-based method for monitoring yeast overexpression strains reveals small-molecule targets in TOR pathway. Nat Chem Biol 2006; 2:103-9; PMID:16415861; https://doi.org/10.1038/nchembio762

[49] van Bruggen HW. Monograph of the genus Aponogeton (Aponogetonaceae). Bibliotheca Botanica 137. Stuttgart, Germany: Schweizerbart'sche Verlagsbuchhandlung, 1985.

[50] Gunawardena AN. An overview of programmed cell death research: from Canonical to emerging model species. In: Gunawardena AN, McCabe Paul F, ed. Plant Programmed Cell Death. Switzerland: Springer International Publishing, 2015:1-31

[51] Wertman J, Lord CE, Dauphinee AN, Gunawardena AH. The pathway of cell dismantling during programmed cell death in lace plant (Aponogeton madagascariensis) leaves. BMC Plant Biol 2012; 12:115; PMID:22828052; https://doi.org/10.1186/1471-2229-12-115

[52] Dauphinee AN, Warner TS, Gunawardena AH. A comparison of induced and developmental cell death morphologies in lace plant (Aponogeton madagascariensis) leaves. BMC Plant Biol 2014; 14:389; PMID:25547402; https://doi.org/10.1186/s12870-014-0389-x

[53] Minina EA, Filonova LH, Fukada K, Savenkov EI, Gogvadze V, Clapham D, Sanchez-Vera V, Suarez MF, Zhivotovsky B, Daniel G, et al. Autophagy and metacaspase determine the mode of cell death in plants. J Cell Biol 2013; 203:917-27; PMID:24344187; https://doi.org/10.1083/jcb.201307082

[54] Takatsuka C, Inoue Y, Matsuoka K, Moriyasu Y. 3-methyladenine inhibits autophagy in tobacco culture cells under sucrose starvation conditions. Plant Cell Physiol 2004; 45:265-74; https://doi.org/10.1093/pcp/pch031

[55] Sarkar S, Carroll B, Buganim Y, Maetzel D, Ng AH, Cassady JP, Cohen MA, Chakraborty S, Wang H, Spooner E, et al. Impaired autophagy in the lipid-storage disorder Niemann-Pick type C1 disease. Cell Reports 2013; 5:1302-15; PMID:24290752; https://doi.org/10.1016/j.celrep.2013.10.042

[56] Gunawardena AHLAN, Navachandrabala C, Kane M, Dengler NG. Lace plant: a novel system for studying developmental programmed cell death. In: Jaime ATdS, ed. Floriculture, ornamental and plant biotechnology Middlesex, UK: Global Science Books, Ltd, 2006:157-62

[57] Pasternak T, Tietz O, Rapp K, Begheldo M, Nitschke R, Ruperti B, Palme K. Protocol: an improved and universal procedure for whole-mount immunolocalization in plants. Plant Methods 2015; 11:50; PMID:26516341; https://doi.org/10.1186/s13007-015-0094-2